24th International Middle East Power Systems Conference (MEPCON), Mansoura University, Egypt 19-21 December 2023

Non-linear PI Controller for Frequency Control of an Islanded Microgrid

H.E. Keshta
Department of Electrical Engineering, Faculty of Engineering at Shoubra, Benha University, Cairo, Egypt
hossam.keshta@feng.bu.edu.eg

Amal Sami Khalil
Department of Electrical Engineering, Faculty of Engineering at Shoubra, Benha University, Cairo, Egypt
Amal.sami.aboarab@gmail.com

M.A. Ebrahim
Department of Electrical Engineering, Faculty of Engineering at Shoubra, Benha University, Cairo, Egypt
mohamed.mohamed@feng.bu.edu.eg

***Abstract*—Islanded Microgrids (MGs) have low inertia, which leads to faster frequency dynamics, and as a result, effective Load Frequency Control (LFC) is required to maintain the frequency within its permitted ranges under different operating scenarios. Typically, conventional linear fixed-gain PI controllers are employed for MG control. In this article, a non-linear variable-gain PI controller is proposed to boost the dynamic performance of a stand-alone MG. The structure of this proposed controller consists of a non-linear function of relative error (e) and the change of error (Δe) values connected with a conventional PI controller. Furthermore, the paper utilizes the TS optimization technique to finely adjust the parameters of the presented controllers. To measure the effectiveness of the suggested controller, the system is exposed to various disturbances such as change in load and weather conditions using MATLAB / Simulink software. The obtained simulation results demonstrate that the proposed controller outperforms the conventional PI controller in terms of maximum overshoot and settling time.**

Keywords—Microgrid, Load Frequency Control, Non-Linear PI Controller, Variable Gain, Transit search Optimization Algorithm.

List of abbreviations

Abbreviation	Definition
DG	Distributed Generation
HRES	Hybrid Renewable Energy Sources
LFC	Load Frequency Control
MGs	Microgrids
MPPT	Maximum Power point tracking
N-DPID	Non-linear discrete proportional integral derivative
PCC	Point of Common Coupling
PLL	Phase-Locked Loop
PMSG	Permanent- Magnet Synchronous Generator
RESs	Renewable Energy Resources
SPWM	Sinusoidal Pulse Width Modulation
TS	Transit Search Algorithm
WECS	Wind Energy Conversion System

I. Introduction

Generating electricity from fossil fuels, natural gas, and coal has significant limitations and environmental impacts, such as the depletion of the fossil fuels, contribution of greenhouse gases and carbon emissions, which lead to global warming and climate change [1]. According to these environmental issues, the world is moving towards green alternative resources such as RESs to meet the increase in electric power demand while reducing pollution. MGs are small scale power system that can effectively integrate various sources of DG, especially RESs such as wind turbines and solar energy [2]. MGs can operate in two modes, namely grid-connected and isolated modes [3].

The islanded MGs have low inertia, which leads to frequency fluctuation and stability problems under the unpredictable nature of RESs caused by continued variation of solar irradiance and wind speed over time [4]. So, isolated MGs must be equipped with an effective and efficient control strategy to keep the frequency within acceptable limits. In past literature associated with MGs, conventional PI controllers [5, 6] have been utilized as they are simple in structure and adequate in performance, but these conventional controllers are not able to operate efficiently over a wide range of operating conditions for non-linear processes. Non-linear variable-gain PI controllers have been developed to avoid and overcome problems that arise using conventional linear PI controllers [7]. A non-linear PI controller with a non-linear function relative to error and reference signal is introduced in [8]. In [9], the author employed a N-DPID controller to achieve MPPT for a photovoltaic system. In this study, a non-linear variable-gain PI controller is proposed with a modern non-linear gain function of error (e) and change of error (Δe) signals to enhance the frequency response over different disturbances. If the relative error is large, the non-linear gain will be large, causing the control signal to increase exponentially. Conversely, decreasing relative error results in an exponential reduction in the control signal.

The primary objectives of this article are: (i) introducing an advanced control strategy for enhancing the dynamic performance of islanded MG under different scenarios. (ii) The proposed non-linear PI controller with a new non-linear function is introduced and compared with the conventional fixed-linear gain PI controller under various disturbances. (iii) tuning the parameters of the proposed controller using a modern optimization algorithm named TS optimization technique.

This article can be divided into several sections, as follows: Section 2 introduces the analysis and modelling of MG. The proposed control strategy is discussed in section 3.

979-8-3503-5846-9/23/$31.00 ©2023 IEEE

The optimization algorithm technique is presented in Section 4. The system dynamic performance derived from non-linear PI controller is compared with conventional linear PI controller under various scenarios, and the obtained results are shown in Section 5. Ultimately, the conclusion is summarized in Section 6.

II. SYSTEM DESCRIPTION

The proposed Micro-Grid comprises of HRES such as a photovoltaic system, wind energy system, and biomass system, all of which are connected to an AC bus through power electronics converters, as shown in Fig. 1. The photovoltaic, wind, and biomass systems are designed to output 1 MW, 1.5 MW and 3.5 MW, respectively. All these RESs contribute to supplying 4 MW AC loads, which is also connected to the AC bus.

III. SYSTEM MODELING

A. *Photovoltaic Subsystem Model:*

Solar radiation and temperature are the two main variables that affect how well solar cells operate. The efficiency and capacity of PV units drop when the temperature exceeds the normal value of 25 °C, although an increase in solar radiation increases the amount of energy produced and, consequently, the PV efficiency. The PV cell can be represented using the one-diode model, as shown in Fig.2. The PV electrical mathematical expression is given by Eq. (1).

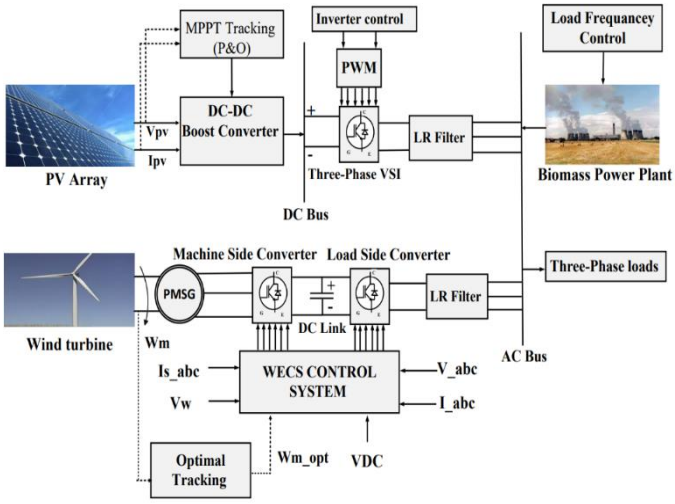

Fig. 1: The proposed micro-grid structure

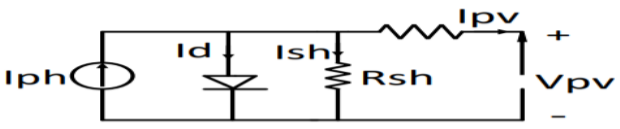

Fig. 2: PV cell equivalent circuit

$$I_{pv} = I_{ph} - I_0(\exp(\frac{q}{KT}(V_{pv} + I_{pv}R_{se})) - 1) - \frac{(V_{pv} + I_{pv}R_{se})}{R_{sh}} \quad (1)$$

where, *Ipv* and *Vpv* are PV cell output voltage and current, respectively; *Iph* is the current generated by the incident light; *Io* is the saturation current of the diode; *q* is electron charge ; *k* is Boltzmann's constant; *T* is ambient temperature; *Rse* is the series resistance of the PV cell; *Rsh* is the shunt resistance of the PV cell.

As shown in Fig.1. The PV model comprises of two essential parts, namely the DC-DC boost converter and the voltage source inverter. DC-DC boost converter is responsible for achieving MPPT, while the inverter is responsible for controlling the active power supplied and the DC-Link voltage.

The PV three phase inverter control strategy is shown in Fig. 3. The control technique applied to the inverter consists of two main cascaded loops, namely current control loop (inner loop) and voltage control loop (outer loop). The purpose of the outer control loop is to control the dc-link voltage, while inner control loop regulates the current [10]. The dq control structure is implemented for the transformation from abc to dq values. The PLL is used to determine the phase angle used for the abc to dq transformation module.

The following equations are obtained by applying KVL at the inverter output and transforming the equation from abc to dq quantities using the Park and Clark transformations.

$$u_d = V_d - E_d - Lwi_q \quad (2)$$

$$u_q = V_q - E_q + Lwi_d \quad (3)$$

The inverter is triggered using SPWM. The relationship between the modulation index, m, the DC link voltage, Vdc, and the inverter output voltages can be expressed as:

$$V_d = m_d \frac{V_{dc}}{2}, \text{and} V_q = m_q \frac{V_{dc}}{2} \quad (4)$$

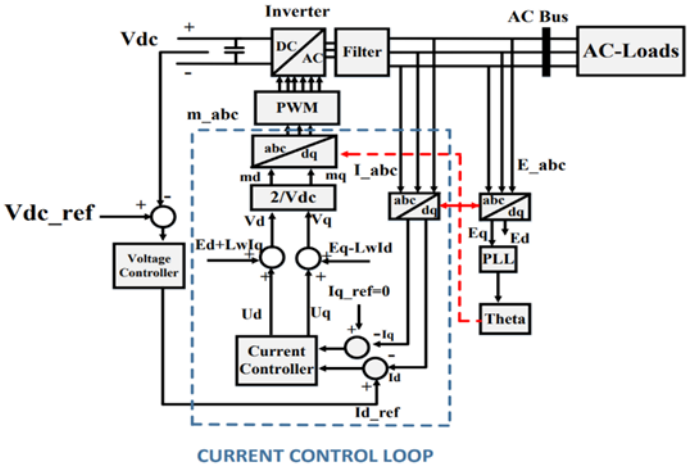

Fig. 3: The PV three phase inverter control strategy

B. *Wind Energy Subsystem Model:*

The WECS shown in Fig. 4, consists of a mechanical part (aerodynamic system) and an electrical part (PMSG with back-to-back converters).

B.1 Mechanical Part of WECS:

The wind turbine mechanical power is given as follows:

$$P_m = \frac{1}{2}\pi\rho R_r^2 C_p V_w^3 \quad (5)$$

Where, ρ is the density of air (kg/m^3), R_r is the wind turbine rotor radius, C_p is the power coefficient and is a

function of tip speed ratio (λ) and the pitch angle (β), is the wind speed (V_w).

$$C_p = c_1\left[\frac{c_2}{\lambda_i} - c_3\beta - c_4\right]e^{\left(\frac{-c_5}{\lambda_i}\right)} + c_6\lambda \tag{6}$$

The expression of the power coefficient C_p is given as follows:

$$\frac{1}{\lambda_i} = \frac{1}{\lambda + 0.08\beta} - \frac{0.035}{\beta^3 + 1} \tag{7}$$

Where, c_1 to c_6 represent the characteristic coefficients of wind turbine.

The tip speed ratio (λ) and mechanical torque (T_m) are calculated as follows:

$$\lambda = \frac{\omega_t R}{V_w} \tag{8}$$

$$T_m = \frac{P_m}{\omega_t} \tag{9}$$

Where, ω_t is the rotational speed (rad/sec)

B.2 Electrical Part of WECS:

As described in Fig.1, the PMSG is connected to back-to back converters, namely machine side converter and load side converter with a DC shunt capacitor connected between them. The machine side converter is responsible for maximizing the output power by controlling wind turbine shaft speed. While load side converter is responsible for regulating the DC link voltage as the PV three phase voltage source converter [12]. The control strategy of machine side converter is shown in Fig.4.

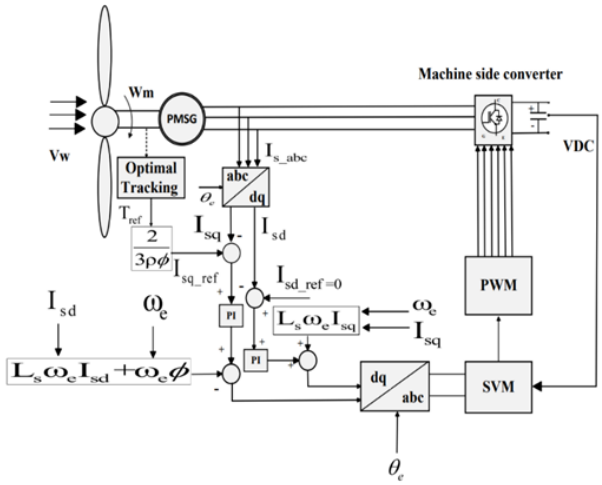

Fig. 4: The control strategy of wind turbine machine side converter

The mathematical expression of the electromagnetic torque (T_e) is given as follows:

$$T_e = \frac{3}{2}pI_{sq}((L_d - L_q)I_{sd} + \phi) \tag{10}$$

Where, p is the number of pole pairs, I_{sq} , I_{sd} are the quadrature and direct components of the currents respectively , L_d , L_q are the direct and quadrature axes inductances respectively, ϕ is the magnetic flux. For surface mounted PMSG, ($L_d = L_q$). Thus, the electromagnetic torque equation will become as follows:

$$T_e = \frac{3}{2}\rho I_{sq}\phi \tag{11}$$

From the above equation, the electromagnetic torque can be controlled through q-axis current (I_{sq}).Consequently, the speed can also be controlled through this q-axis current.

IV. SYSTEM CONTRL DESIGN

Linear fixed-gain PI controllers are characterized by their simple construction and adequate performance, but these conventional controllers provide the finest performance only during certain operating ranges. Therefore, they can't provide the desired performance for non-linear processes with a wide range of operating conditions [13].

A linear fixed-gain PI controller's mathematical structure is typically described as follows:

$$u(t) = k_p\, e(t) + k_i \int_0^t e(t)\,dt \tag{12}$$

Where, $u(t)$ represents control signal, k_p and k_i are proportional and integral gains, respectively, $e(t)$ represents error signal.

The non-linear variable gain PI controller is proposed to overcome the drawbacks of the conventional PI controller [14]. It consists of non-linear gain function of error (e) and change of error (Δe) signals cascaded with a linear fixed-gain PI controller.

The mathematical structure of the non-linear variable gain PI controller is introduced as follows:

$$u(t) = \left(k_p\, e(t) + k_i \int_0^t e(t)\,dt\right) k(e,\Delta e) \tag{13}$$

$$u(t) = k_p\, k(e,\Delta e)\, e(t) + k_i\, k(e,\Delta e) \int_0^t e(t)\,dt \tag{14}$$

$$k_p\, k(e,\Delta e) = k_p' \tag{15}$$

$$k_i\, k(e,\Delta e) = k_i' \tag{16}$$

$$u(t) = k_p'\, e(t) + k_i' \int_0^t e(t)\,dt \tag{17}$$

$$k(e,\Delta e) = \alpha - \left(\frac{\exp(\beta_1 \times e) + \exp(-\beta_2 \times \Delta e)}{2}\right) \tag{18}$$

Where, $k(e,\Delta e)$ is the non-linear gain function and α, β_1, β_2 are the parameters of the designed controller. Block diagram of non-linear PI controller is shown in Fig. 5. This controller structure differs from other non-linear controllers in previous literature in that it consists of non-linear gain, which is a function of error (e) and the change of error (Δe). In this manner, the control signal is greatly affected by the error signal.in other words, when the relative error decreases, the control signal exponentially decreases. But in case of large error, the control signal exponentially increases, which in turn retains the system output to its reference value rapidly

[15]. The parameters' values of the non-linear gain function and fixed-linear PI controller gains are shown in the table 1

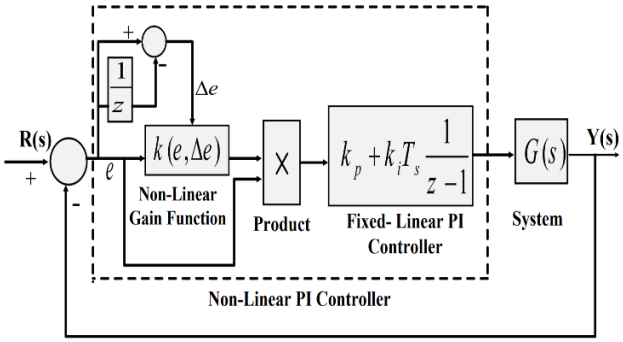

Fig. 5: Non-linear PI controller block diagram

Table 1: The non-linear gain function and fixed-linear PI controller gains

Parameter	Value
Non-linear controller parameter (α)	2.57
Non-linear controller parameter (β_1)	0.2
Non-linear controller parameter (β_2)	0.01
Proportional gain of pi controller (k_p)	75.2522
Integral gain of pi controller (k_i)	7.18278

V. OPTIMIZATION TECHNIQUE

The gains of PI controllers are optimized using advanced optimization technique called TS algorithm, which established on the method of exoplanet exploration by measuring the amount of brightness from the star during specific intervals, if there is a noticeable reduction in brightness, this points to the transit of a planet in front of the star [16]. The flow chart of the TS algorithm is shown in Fig. 6. According to this flow chart, there are five phases used for carrying out the TS optimization technique. Namely, Galaxy phase, Transit phase, Planet phase, neighbor phase and exploitation phase.

A. Galaxy Phase

$$\begin{aligned} L_{R,i} &= L_G + D - N, i = 1,.....,(SN \times n_s) \\ D &= \{c_1 L_{R,i} - L_r\} \rightarrow if\ Z = 1 \\ D &= \{c_1 L_{R,i} + L_r\} \rightarrow if\ Z = 2 \end{aligned} \quad (19)$$

where, $L_{R,i}$ is the galaxy's habitable zone, L_G is randomized location of galaxy's centre, L_r is randomized location in the search area, N is the nnoise, SN is the signal-to-noise ratio, n_s is host stars number, c_1 is a randomized number, and c_2 is a randomized vector. The two coefficients between 0 and 1, respectively. Z is the zone parameter may be equal 1 or 2, D represents the difference between the galaxy centre and the selected location under study.

$$\begin{aligned} L_{S,i} &= L_{R,i} + D - N, i = 1,.....,n_s \\ D &= \{c_4 L_{R,i} - c_3 L_r\} \rightarrow if\ Z = 1 \\ D &= \{c_4 L_{R,i} + c_3 L_r\} \rightarrow if\ Z = 2 \\ N &= [c_5]^3 L_r \end{aligned} \quad (20)$$

Where , $L_{S,i}$ is the star location , c_3 and c_4 are randomized numbers between 0 and 1 while c_5 is randomized vector which is also between 0 and 1.

B. Transit Phase

$$\begin{aligned} L_i &= \frac{R_i / n_s}{(d_i)^2}, i = 1,.....,n_s, R_i \in 1,.....,n_s \\ d_i &= \sqrt{(L_S - L_T)^2}, i = 1,.....,n_s \end{aligned} \quad (21)$$

Where, L_i is the star, i illumination, R_i the rank of the star i , d_i is the distance between the star i and the telescope , L_T is the telescope location. The illumination received from the star is updated by changing the value of L_S according to the below equation.

$$\begin{aligned} L_{S,new,i} &= L_{S,i} + D - N, i = 1,.....,n_s \\ D &= c_6 L_{S,i} \\ N &= [c_7]^3 L_S \end{aligned} \quad (22)$$

Where, $L_{S,new,i}$ is the new location of the star i , c_6 is a randomized number between -1 to 1 and c_7 is a randomized vector between 0 and 1. The new illumination $L_{i,new}$ from the star can be calculated by the following equation.

$$\begin{aligned} L_{i,new} &= \frac{R_{i,new} / n_s}{(d_{i,new})^2} \\ d_i &= \sqrt{(L_{S,new,i} - L_T)^2} \end{aligned} \quad (23)$$

If there is a reduction in the new illumination received from the star compared to the previous illumination, this points to a transit of planet in front of the star. In contrast, if the new illumination received from the star is the same of the previous illumination, this means that no transit has occurred.

$$\begin{aligned} &\text{If } L_{S,new,i} < L_i \rightarrow P_T = 1 \\ &\text{If } L_{S,new,i} \geq L_i \rightarrow P_T = 0 \end{aligned} \quad (24)$$

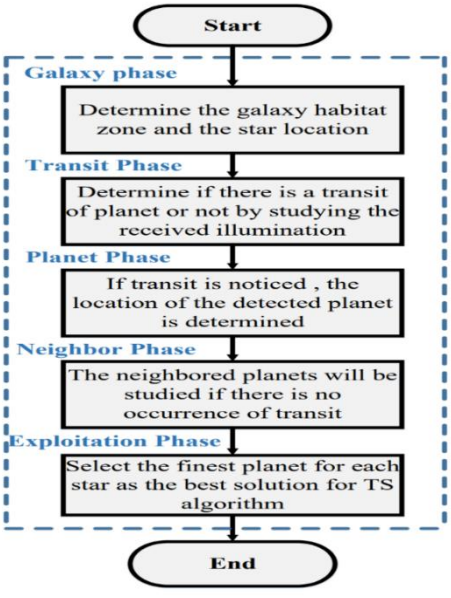

Fig. 6: Flow chart of TS algorithm

C. Planet Phase

When, $P_T = 1$

$$L_z = (c_8 L_T + R_L L_{S,i}) / 2, i = 1, ..., n_s \quad (25)$$

Where, L_z is the location of detected planet, R_L is the luminance ratio and c_8 is a randomized number between 0 and 1.

D. Neighbor Phase

When, $P_T = 0$

$$L_z = (c_{11} L_{S,new} + r_L c_{12}) / 2 \quad (26)$$

Where, L_z is the location of neighbor planet, $L_{S,new}$ is the host star of neighbor planet c_{11} , and c_{12} are randomized number between 0and 1, r_L is a random location.

E. Exploitaion Phase

In this phase, the finest planet is chosen for each star as the best solution.

VI. SIMULATION RESULTS AND DISCUSSION

To prove the effectiveness of the proposed controller in improving frequency response for islanded MG, the system is subjected to some various scenarios and disturbances using MATLAB / Simulink software, then the obtained results are compared with conventional linear PI controller.

A. Scenario 1: Three Phase Short Circuit

In this scenario, a three-phase short circuit fault is applied to PCC at 5 sec and cleared at 5.1 sec. The occurrence of SC fault results in a reduction in active output power from 4MW to 1MW and an increase in electric fault current, which in turn causes a drop in electrical voltage and frequency as there is a direct relation between each other.

As shown in Fig.7, the proposed non-linear PI controller, responds effectively to the SC disturbance and retains the frequency to its reference value within acceptable ranges by reducing the overshoot of the system's frequency response as compared with conventional PI controller. In case of conventional PI controller, the frequency deviates from 47 Hz to 52 Hz, while in case Non-linear PI controller, the frequency deviates from 49Hz to 50.65 Hz.

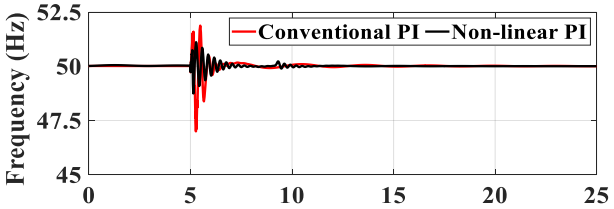

Fig. 7: Frequency response according to three-phase SC fault

B. Scenario 2: Sudden Load Change

The mismatch between the power generated and power consumed by loads results in a variation in the speed of the generator. When the load increases, the generator's speed slows down causing a reduction in the frequency. Conversely, if the load decreases, the frequency increases. In this scenario the load demand suddenly increased by 25% from 4MW to 5MW at 5 sec and then decreased from 5MW to 4MW at 15 sec. As shown in Fig.8, An increase in load can cause a drop in frequency to 49.7 Hz,49.57Hz for Non-linear PI controller and conventional PI controller, respectively. At 15 sec, the load reduction causing an increase in frequency to 50.3Hz, 50.5Hz for Non-linear and conventional PI controllers, respectively. In case of load reduction, the settling time of frequency response are 2 sec for Non-linear PI controller and 6 sec for conventional PI controller.

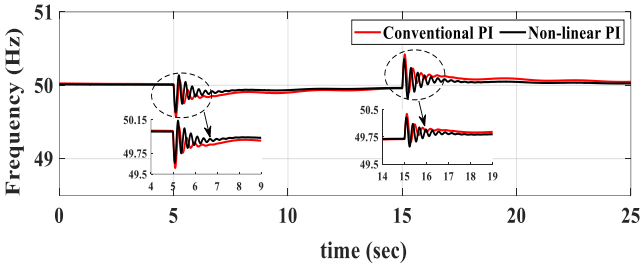

Fig. 8: Frequency response according to sudden load change

C. Scenario 3: Sudden Irradiance change

The power generated from the PV system depends essentially on the solar irradiance. As shown in Fig.9, the solar irradiance is suddenly decreased from 1000W/m^2 to 250W/m^2 at 5 sec causing a reduction in the electrical output power from 1MW to 0.2445MW. According to the mismatch between load and generation, the frequency is reduced to 49.75Hz,49.6Hz for Non-linear and conventional PI controllers, respectively. At 15 sec, there is a sudden increase in the solar irradiance from 250W/m^2 to 1000 W/m^2 causing an increase in frequency to 50.25 Hz ,50.4Hz with settling time 2 sec, 6 sec for Non-linear and conventional PI controller respectively. In Fig.10, the reference dc link voltage of the PV system is 1050V, according to the solar irradiance disturbance at 5sec, the settling time of the pv system dc link voltage response is 2 sec for Non-linear PI controller, 6 sec for conventional PI controller. At 15sec disturbance, the settling time is 2 sec and 6 sec for non-linear and conventional PI controllers, respectively, as shown in Fig. 10 and table 2.

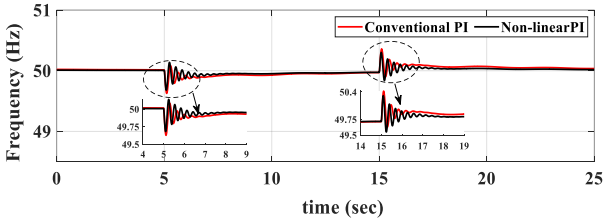

Fig. 9: Frequency response according to sudden irradiance change

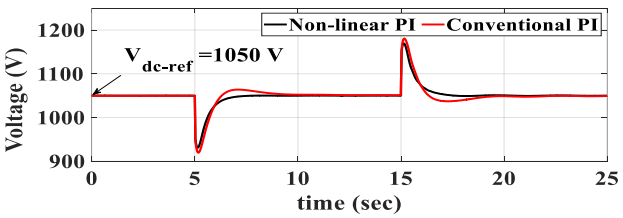

Fig. 10: The DC link voltage of the PV system according to solar irradiance disturbance

D. *Scenario 4: Sudden wind speed change*

As shown in Fig.11, the wind speed is suddenly decreased from 12m/s^2 to 9m/s^2 at 5 sec causing a reduction in the output power from 1.5MW to 0. 44MW.According to this reduction in power, there will be a drop in frequency to 49.78 Hz ,49.6Hz for Non-linear and conventional PI controllers, respectively. At 15 sec disturbances, the frequency deviates from 49.75 Hz to 50.5 Hz for conventional PI controller with settling time 7 sec while, it deviates from 49.87Hz to50.3Hz for Non-linear PI controller with settling time 3 sec as shown in Fig. 11 and table 2.

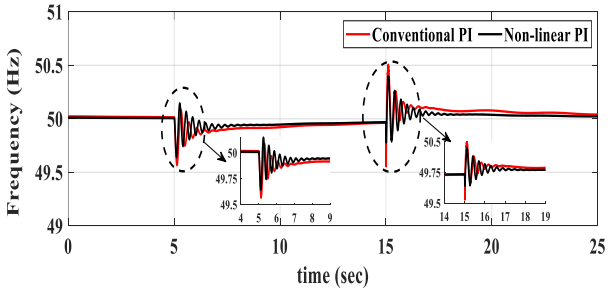

Fig. 11: Frequency response according to sudden wind speed change

Table 2: Comparison between overshoot and settling time of the frequency response in case of Non-linear and Conventional PI Controllers

Scenario	Controller type	Overshoot	Settling time
Three-Phase Short Circuit Fault at 5 sec	Non-linear PI	0.65 Hz	2 sec
	Conventional PI	2 Hz	6 sec
Sudden Load Change at 15 sec	Non-linear PI	0.3 Hz	2 sec
	Conventional PI	0.5 Hz	6 sec
Sudden Irradiance Change at 15 sec	Non-linear PI	0.25 Hz	2 sec
	Conventional PI	0.4 Hz	6 sec
Sudden Wind Speed Change at 15 sec	Non-linear PI	0.3 Hz	3 sec
	Conventional PI	0.5 Hz	7 sec

VII. CONCULSION

A non-linear variable-gain PI controller is proposed in this paper to enhance the frequency response of an isolated micro-grid. The five parameters of the proposed non-linear PI controller are optimally tuned by an advanced meta-heuristic technique called TS optimization algorithm. The system is subjected to various disturbances, such as short circuit fault occurrence, variations in load demand and changes in weather conditions to verify the performance of the proposed controller.

The results obtained from simulation demonstrate that a non-linear variable-gain PI controller provides better dynamic performance with respect to maximum overshoot and settling time, as compared to a linear fixed-gain PI controller, under all applied disturbances.

REFERENCES

[1] G. S. Chaurasia., A. K. Singh, S. Agrawal, and N. K. Sharma, "A meta-heuristic firefly algorithm based smart control strategy and analysis of a grid connected hybrid photovoltaic/wind distributed generation system," Solar Energy, vol. 150, 2017, pp. 265-274.

[2] H. E. Keshta, E. M. Saied, O. P. Malik, F. M. Bendary, and A. A. Ahmed, "Fuzzy PI controller-based model reference adaptive control for voltage control of two connected microgrids," IET Generation, Transmission & Distribution, vol. 15, no. 4, 2021, pp. 602-618.

[3] A. E. Khalil, T. A. Boghdady, M. H. Alham, and D. K. Ibrahim, "Enhancing the Conventional Controllers for Load Frequency Control of Isolated Microgrids Using Proposed Multi-Objective Formulation via Artificial Rabbits Optimization Algorithm," in IEEE Access, vol. 11, 2023, pp. 3472-3493.

[4] K. I. Annapoorani, V. Rajaguru, S. A. Padmanabhan, K. M. Kumar, , and S. Venkatachalam, "Fuzzy logic-based integral controller for load frequency control in an isolated micro-grid with superconducting magnetic energy storage unit," Materials Today: Proceedings, vol. 58, 2022, pp. 244-250.

[5] R. Dhanalakshmi, “Load Frequency Control of Wind Diesel Hydro Hybrid Power System Using Conventional PI Controller,” European Journal of Scientific Research, vol. 60, no. 4, 2011, pp. 630-641.

[6] N. Kumari, and A. N. Jha, "Frequency Response Enhancement of Hybrid Power System by using PI Controller Tuned with PSO technique," International Journal of Advanced Computer Research, vol. 4, 2014, pp. 2249-7277.

[7] Y. Ren, L. Li, J. Brindley, and L. Jiang, "Nonlinear PI control for variable pitch wind turbine, " Control Engineering Practice, vol. 50, 2016, pp. 84-94.

[8] D. Pathaka, G. Sagara, and P. Gaura, “An Application of Intelligent Non-linear Discrete-PID Controller for MPPT of PV System,” International Conference on Computational Intelligence and Data Science, vol. 167, 2020, pp. 1574–1583.

[9] W. Bai, M. R. Abedi, and K. Y. Lee, "Distributed generation system control strategies with PV and fuel cell in microgrid operation," Control Engineering Practice, vol. 53, 2016, pp. 184–193.

[10] D. Haribabu, A. Vangari and J. N. Sakamuri, "Dynamics of voltage source converter in a grid connected solar photovoltaic system," 2015 International Conference on Industrial Instrumentation and Control, 2015, pp. 360-365.

[11] P. Gajewski, and K. Pieńkowski, “Advanced control of direct-driven PMSG generator in wind turbine system,” Archives of Electrical Engineering, vol. 65, no. 4, 2016, pp. 643-656.

[12] A. H. K. Alaboudy,, A. A. Daoud, S. S. Desouky, and A. A. Salem. "Converter controls and flicker study of PMSG-based grid connected wind turbines." Ain Shams Engineering Journal, vol. 4, no. 1, 2013, pp. 75-91.

[13] Y.X. Su, D. Sun, and B.Y. Duan, " Design of an enhanced nonlinear PID controller," Mechatronics, vol. 15, 2005, pp. 1005–1024.

[14] M. Habbab, A. Hazzab, and A. Alalei, “Real Time Implementation of Nonlinear PI Controller for the Induction Machine Control,” Journal of Fundamental and Applied Sciences, 2019, pp. 1033-1044.

[15] Ş. Akkaya, H. Nak, and A. F. Ergenç, “Design, Analysis and Experimental Verification of A Novel Nonlinear PI Controller,” vol. 18, no. 4, 2017, pp. 876 – 896.

[16] H. S. Das, A. Dey, T. C. Wei, and A. H. M. Yatim, “Transit search: An optimization algorithm based on exoplanet exploration,” Results in Control and Optimization, vol. 7, 2022, pp. 100–127.